A SURVEY OF THE INTERSTELLAR MEDIUM IN EARLY-TYPE GALAXIES. III. STELLAR AND GAS KINEMATICS[1]

NICOLA CAON

Instituto de Astrofísica de Canarias Via Lactea s/n, La Laguna E-38200, Tenerife, Spain; ncaon@ll.iac.es

DUCCIO MACCHETTO

Space Telescope Science Institute 3700 San Martin Drive, Baltimore, MD 21218; macchetto@stsci.edu

AND

MIRIANI PASTORIZA

Instituto de Fisica, UFRGS Av Bento Goncalves 9500, CP 15015 91500, Porto Alegre RS, Brazil; mgp@if.ufrgs.br

ABSTRACT

We present gaseous and stellar kinematics for 14 gas-rich early-type galaxies. Half of the sample exhibit irregular gaseous velocity profiles; gas/star counter-rotation is visible in five galaxies. We also find five counter-rotating stellar cores, while five more galaxies display inner components kinematically decoupled from the main stellar body. We interpret our results as an indication that the ionized gas is of external origin, is generally not in equilibrium, and may have been acquired recently. The merging or accretion events that brought the gas into the galaxy have also affected the stellar kinematics.

Subject headings: galaxies: elliptical and lenticular, cD — galaxies: ISM — galaxies: kinematics and dynamics

1. INTRODUCTION

Several studies (Phillips et al. 1986; Kim 1989; Shields 1991; Buson et al. 1993; Goudfrooij et al. 1994) have shown that more than 50% of elliptical and lenticular galaxies contain a substantial amount of ionized gas. As part of the ESO Key-Program 1-004-43K: "Toward a physical understanding of early-type galaxies," Macchetto et al. (1996, hereafter Paper I) have mapped the ionized gas in a sample of 73 ellipticals and S0s through narrowband images centered at the Hα and [N II] emission lines.

Gas emission was detected in about 3/4 of the sample galaxies, with ionized gas masses ranging from 10^3 to 10^5 $M_\odot$. The line-emitting gas shows a wide range of morphologies and sizes, from small, compact disklike distributions to extended (up to 10 kpc) and complex filamentary structures. The properties of the ionized gas were found to exhibit interesting correlations with the global properties of the host galaxies (see also Goudfrooij 1996).

There is a clear correlation between Hα + [N II] and X-ray luminosities, though some X-ray sources show no ionized-gas emission. This correlation is in line with the model proposed by Sparks & Collier-Cameron (1988) and Sparks, Macchetto, & Golombek (1989), in which thermal electron conduction causes energy to flow from the hot coronal component into the cold gas, exciting it into emission (while cooling the hot gas). The data presented in Paper I show indeed an excellent agreement between the observed Hα + [N II] fluxes and those predicted from the X-ray fluxes using this model.

While the relation between Hα + [N II] luminosities and total B-band magnitudes is very loose, the correlation with the B-band luminosity integrated within the region occupied by the ionized gas is much tighter and clearer.

This suggests the role of hot, post-AGB stars as an additional/alternative ionization mechanism. The ratio between the photon flux produced by hot, old stars, as predicted by the model by Binette et al. (1994), and the photons actually used or needed to ionize the gas, as computed for case B recombination (Osterbrock 1974), is of order unity.

Other possible sources of excitation and ionization are photoionization by hot young stars (Kim 1989; Shields 1991), radiation originating in an active nucleus (Fosbury et al. 1982), and shocks (Heckman et al. 1989).

Which ionization mechanisms are dominant, and whether and how their relative importance changes from one object to another, is still an open issue.

The origin of the ionized gas, too, is a controversial subject. Two of the main scenarios so far proposed are as follows.

Cooling flows.—The ionized gas is the product of cooling flows in which the material lost by stars, heated to high temperatures (~ 1 keV) by Supernovae explosions, cools and condenses into filaments (see Fabian 1994 for a review). However, this scenario cannot account for the remarkable coexistence of gas and dust in the same spatial locations (see Ferrari et al. 1999) and cannot predict the correct energy budget of the gas emission.

External origin.—The gas is accreted from other galaxies during mergers or close encounter events; the ionizing mechanisms above mentioned can fully account for the energy balance. This scenario can explain the coexistence of gas and dust and is supported by the frequent detection of kinematical decoupling between stellar and gaseous kinematics in gas-rich early-type galaxies.

Several studies have shown indeed that in quite a few elliptical and lenticular galaxies the angular momenta of stars and gas are misaligned, or even antiparallel. Bertola et al. (1995) studied a sample of eight lenticular galaxies and found that the gas can present central velocity gradients steeper, equal to, or even shallower than the stellar velocity

NGC 3379

NGC 3489

NGC 3607

NGC 4105

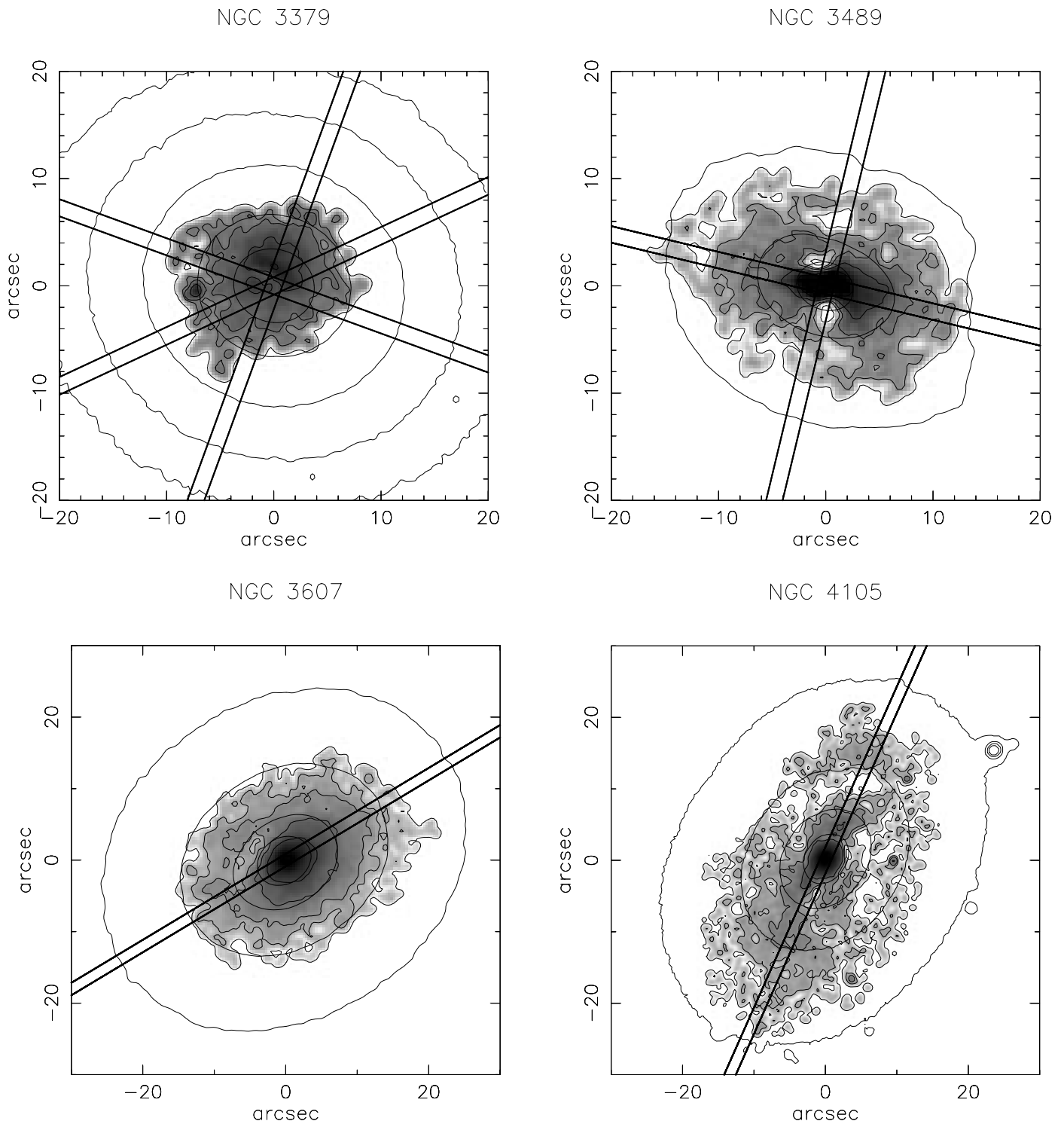FIG. 1.—Positions of the slit superposed on the Hα + [N II] maps and R isophotes (from Paper I)

gradients. In the latter two cases the gas has a significant velocity dispersion, and its rotation does not trace the circular velocity. Zeilinger et al. (1996) studied six gas-rich ellipticals and found a variety of gas kinematics (no comparison with star kinematics was presented, however), from regular rotation curves to peculiar behaviors. In one case, NGC 6868, there is evidence for two gas components counterrotating with respect to each other. Plana et al. (1998) analyzed Perot-Fabry observations of 11 ellipticals and

confirmed the presence of distinct gaseous components in three of their galaxies.

In order to better understand the dynamical status of the gas in early-type galaxies, and its relation with the stellar body, we have carried out a long-slit spectroscopic observational program to measure gas and stellar kinematics in a fair sample of gas-rich ellipticals and S0s. These data provide a direct comparison of the dynamical behavior of gas and of stars, and allow the derivation of information on
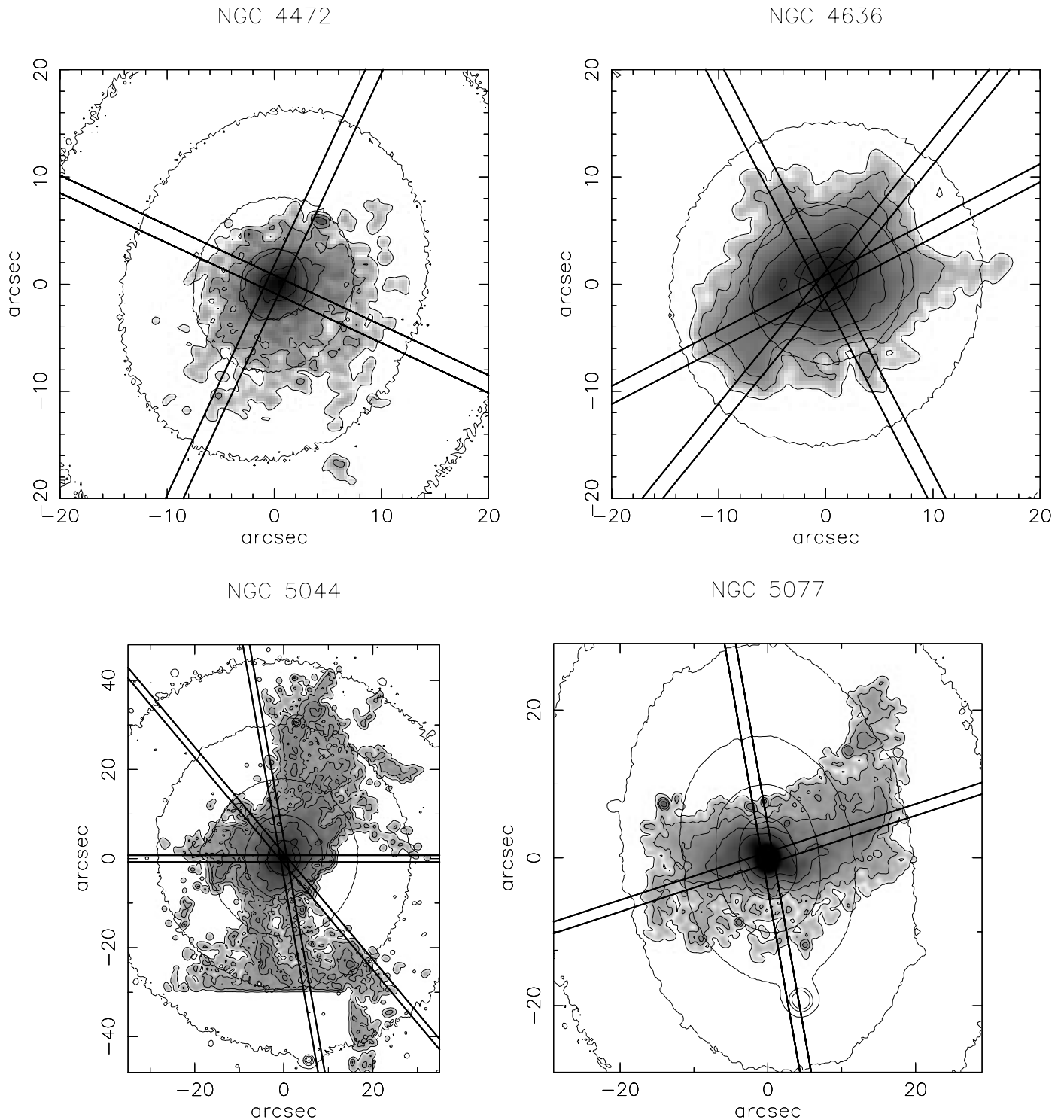
NGC 4472

NGC 4636

NGC 5044

NGC 5077

FIG. 1.—*Continued*

the possible origin of the gas (accretion versus cooling flows). In this paper we present gaseous and stellar velocity curves, and stellar velocity dispersion profiles for 14 of the galaxies in our sample with the brightest and most extended gas distributions, and compare the gas and stellar kinematical characteristics.

This paper is organized as follows. Section 2 presents the observations and the data reduction; §§ 3 and 4 deal with the analysis of the gas and of the stellar kinematics, respectively. Section 5 describes the main characteristics for each

galaxy individually; comparisons with literature data are presented in § 6; finally, in § 7 a general discussion of the results will be made, and conclusions will be drawn.

2. OBSERVATIONS AND DATA REDUCTION

The galaxies presented in this paper have been selected from the sample of elliptical and lenticular galaxies whose ionized gas distribution has been studied by Macchetto et al. (Paper I). We chose the galaxies with the most extended and luminous (in apparent units) gas distribution, which
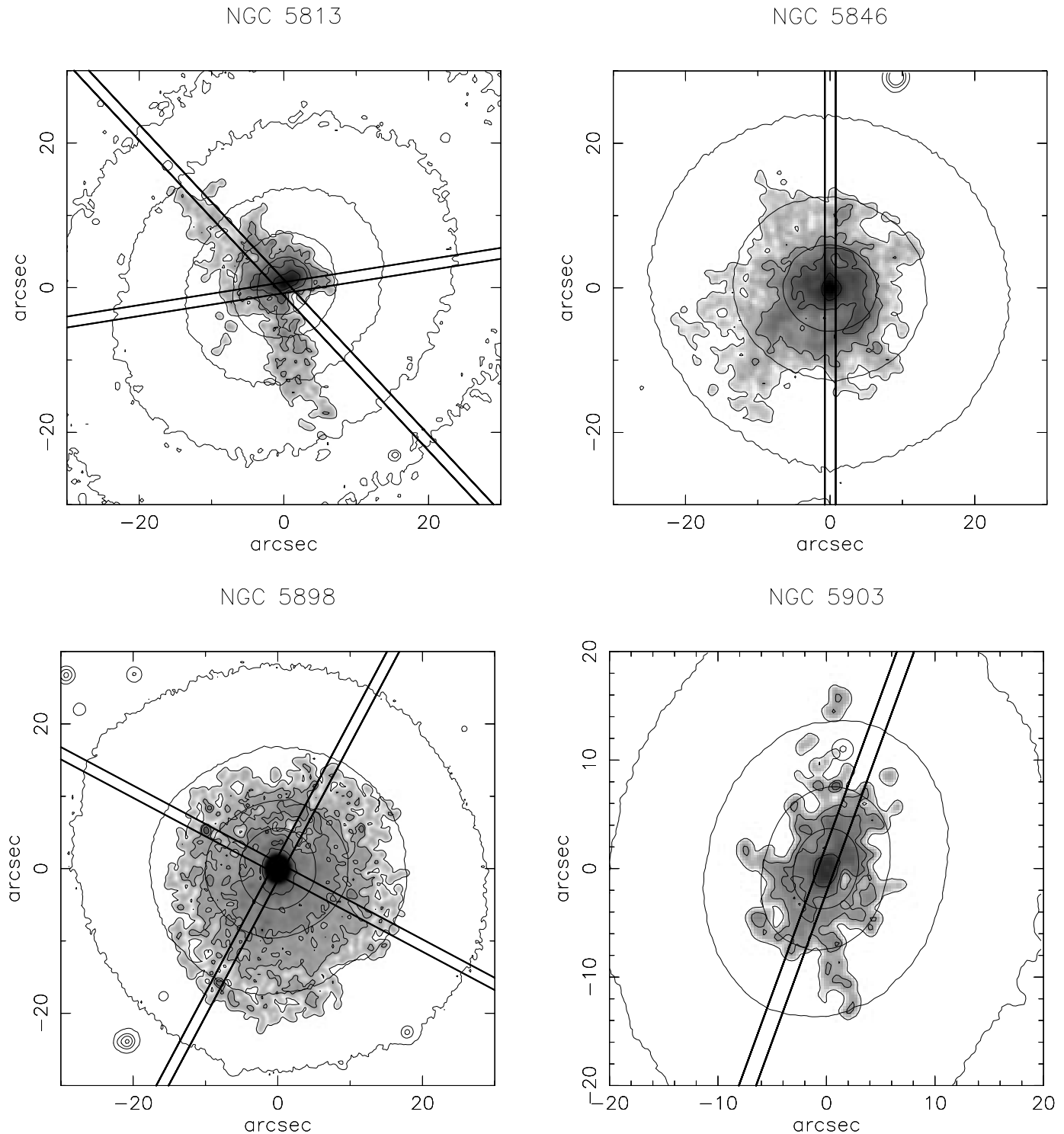
NGC 5813

NGC 5846

NGC 5898

NGC 5903

FIG. 1.—*Continued*

were visible at the time of the observations (excluding some already well-studied objects such as NGC 4486 and NGC 5102). For each galaxy, long-slit spectra were obtained at up to three position angles (P.A.), oriented along the main axes of the gas and/or stellar distributions. (In a few cases, we could only observe a single P.A. due to bad weather).

The positions of the slit, superposed on a $H\alpha + [N\ \textsc{ii}]$ image and R-band isophotes map, are shown in the panels of Figure 1.

The observations were conducted at the ESO 3.6 m telescope on La Silla, Chile, equipped with EFOSC1. In order

to maximize the coverage of the relevant stellar absorption and gaseous emission lines, without compromising the spectral resolution, we used the O150 grism in the range 5140–6900 Å with a dispersion of 3.4 Å pixel^{-1} with CCD 26 (Tektronix 512×512 pixels). The spatial scale is $0\rlap{.}''61$ pixel^{-1}; the slit length was $3\rlap{.}'1$, while its width was fixed to $1\rlap{.}''5$, approximately the average seeing. The actual spectral resolution has been determined using both the He + Ar lines in the arc spectra, and unblended sky lines present in the exposures; the agreement among the measurements is excellent, giving 2.15 pixels FWHM (corresponding to
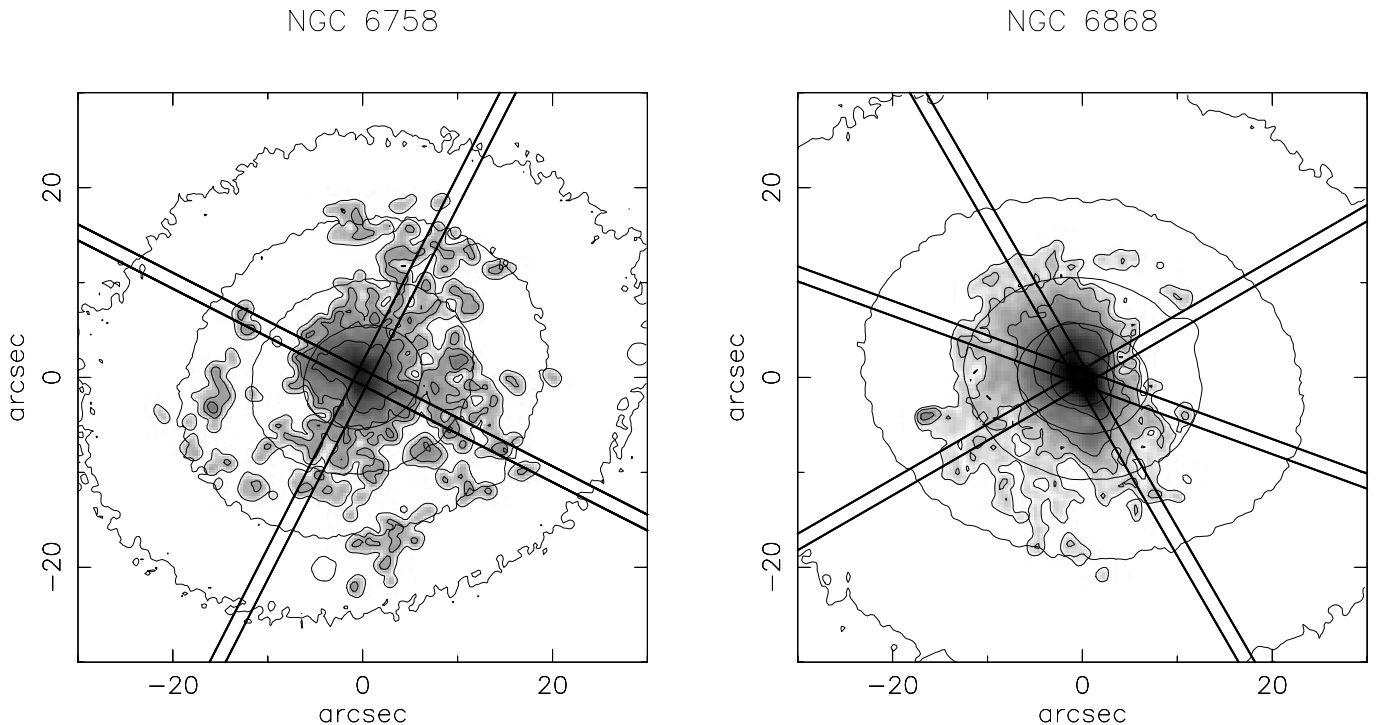
NGC 6758

NGC 6868

FIG. 1.—*Continued*

about 365 km s^{-1} for the above spectral range). This value is also consistent with the width of stellar absorption lines in the kinematic template stars. Normally, two spectra of 40–45 minutes for each position angle were obtained, in order to increase the signal-to-noise ratio and to facilitate the removal of cosmic-ray events. The seeing varied from 1″2–1″8. The log of the observations, together with the main parameters of the objects, is shown in Table 1.

Since for the purposes of our work we do not need a very accurate determination of the velocity zero points, which could shift because of instrumental flexure, we did not take arc spectra bracketing galaxy exposures. However, the stability of the instrument has been checked by measuring the position of the sky emission lines present in the galaxy spectra; the results show that, among all galaxy exposures, the relative shift is always less than a few tenths of a pixel, with a rms of about 0.15 pixels ($\simeq 25$ km s^{-1}). We also checked the correct alignment of the CCD Y-axis with the dispersion direction by tracing, for each spectrum, the position of the centroid of the galaxy or star light distribution along each detector row. No systematic misalignment was found, with the tilts never larger than 0°05 (0.5 pixels from bottom to top).

Several kinematic templates (giant stars in the spectral type range K0–K4 III, with rotation velocity less than 20 km s^{-1}) and spectrophotometric standards were observed at the beginning and the end of each night.

We used standard IRAF tasks to process the spectra. The mean bias level was subtracted from each spectrum, which was subsequently divided by a normalized dome flat-field map to remove pixel-to-pixel variations in sensitivity. No dark current was subtracted, since we found that the dark current level is very low and does not show any variations across the frame. The averaged twilight flat has been used to correct for the response along the slit.

Cosmic-ray events were removed by standard IRAF tasks. Some fainter events, relative to the local background,

remained undetected but were found by inspecting the two exposures of each pair at the same position angle, and interpolated over.

The centroids of the brightest, nonsaturated lines in the He + A comparison spectra were measured to obtain the wavelength calibration (with a scatter of about 0.15 Å), and to map the line curvature. Each galaxy and standard star spectrum was rectified and rebinned to a logarithmic wavelength scale with constant step of 86 km s^{-1} (half the original pixel size). We tested the accuracy of the wavelength scale by applying these steps to the calibration spectrum itself and cross-correlating different spatial cuts with the central cut taken as a reference. Relative velocities agreed within ± 10 km s^{-1}.

Finally, for each galaxy the sky spectrum was determined by taking the median value within two windows 10–20 pixels wide at both ends of the slit and subtracted out, after checking that no line emission was present in these regions. While this method implies an oversubtraction of the sky level, as a fraction of the galaxy spectrum is also removed, it is not expected to affect significantly the kinematical profiles (see discussion in Saglia et al. 1993).

Pairs of spectra taken along the same position angle were averaged together, after correcting for the small misalignments of the spectra with respect to the dispersion axis and the small relative shifts along the spatial axis whenever necessary.

3. GAS KINEMATICS

We mostly used the [N II] $\lambda6583.6$ line, usually the strongest and most prominent in the spectral range covered, to derive the gas kinematics. Given the complex spectral pattern in the Hα and [N II] doublet region, we fitted interactively, at each position, a Gaussian profile to the [N II] $\lambda6583.6$ line rather than rely on more sophisticated, automated methods. The IRAF task "splot" was used. In a few cases, we restricted the fit to the peak and red side of

[N II] λ6583.6, to minimize the influence of the adjacent Hα stellar absorption line, which can distort the shape of the blue wing.

We also measured, whenever the signal was good enough, Hα, [N II] λ6548.1 and the [S II] doublet (which is generally blended and was fitted as a sum of two Gaussians with equal FWHM). In general, these lines were found less useful for determining the gas kinematics: the Hα gaseous emission is usually buried in the stellar absorption line, and only in a few objects it is clearly visible; [N II] λ6548.1 is faint and overlaps the blue wing of the Hα absorption line; the [S II] lines are weaker than [N II] λ6583.6, and only in a few objects we could obtain good determinations of their position. Whenever two or more lines could be reliably measured at a given location, we computed the weighted average of the corresponding radial velocities.

In the outer regions, several rows were averaged together, with binning size increasing outward, to increase the signal-to-noise ratio.

The Gaussian fit algorithm in "splot" also provides an estimate of the uncertainties in the derived quantities by means of Monte Carlo simulation. A number of simulations of the spectrum are created by adding random Gaussian noise, based on a statistical model of the data; for each simulation, a fit is performed keeping fixed the background level. The width of the distribution of the derived parameters then gives an estimate of the associated uncertainties.

Further sources of error are the determination of the background level, and possible distortions and asymmetries of the line profile.

A more realistic estimate of the uncertainties can be obtained from measurements made with different background levels, or from the scatter among different spectral lines. These uncertainties depend on the local continuum and line strength and can be as large as 50–100 km s^{-1}; they are included in our error bars.

Because of the resolution of our spectra (comparable to or larger than the typical gas dispersion velocity), and because line widths are very sensitive to the exact background level adopted (much more so than the centroid of the line is), we could not produce gas velocity dispersion profiles for the spectra. However, in a few spectra, where the line widths are significantly higher than the instrumental width and show good agreement among different lines, we can give at least an estimate of the gaseous central velocity dispersion.

4. STELLAR KINEMATICS

A cross-correlation algorithm, working in pixel space, has been used to derive the stellar kinematics. We followed the method described by Dalle Ore et al. (1991), to which we refer the reader for more details. Briefly, for each galaxy and template spectrum, a polynomial was fitted to the continuum and subtracted out. We have experimented with differ-

TABLE 1
LOGBOOK OF OBSERVATIONS AND GALAXY PARAMETERS

Identification	Type	B_T	$F_{H\alpha + [N\ II]}$ $(10^{-14}$ ergs s^{-1} cm$^{-2})$	Distance (Mpc)	P.A. (deg)	Exposure Time (minutes)
1995 May						
NGC 3607......	S0	10.79	7.8	14.7	121	2 × 40
NGC 4105......	S0	11.34	13.5	34.9	156	2 × 40
NGC 5044......	E0	11.67	39.2	52.2	10	2 × 40
					40	2 × 40
					90	40
NGC 5077......	S0	12.21	16.3	52.2	10	2 × 40
					108	2 × 40
NGC 5813......	E1	11.42	11.3	34.9	43	2 × 45
					99	45
NGC 5846......	S0	10.91	28.0	34.9	0	2 × 40
NGC 5903......	E3/S0	11.74	5.2	44.3	60	2 × 40
NGC 6758......	E2	12.31	6.8	58.8	63	2 × 40
					153	2 × 40
NGC 6868......	E3/S0	11.49	27.6	48.6	30	2 × 40
					70	40
					120	2 × 40
1996 Mar						
NGC 3379......	E0	10.18	10.1	14.5	25	2 × 45
					115	2 × 45
					160	2 × 45
NGC 3489......	S0/Sa	11.15	51.9	9.2	76	2 × 45
					166	45
NGC 4472......	E1/S0	9.33	17.3	21.3	65	2 × 40
					155	2 × 40
NGC 4636......	E0/S0	10.43	21.4	21.3	27	2 × 45
					117	2 × 45
					141	2 × 40
NGC 5898......	S0	11.92	16.4	44.3	62	2 × 40
					152	2 × 45

ent polynomial degrees and found that degrees around 20 provided the best fit: lower degrees were unable to follow adequately the continuum shape, while higher degrees might present unwanted oscillations.

The resulting spectrum was cross-correlated with the spectrum of the kinematic template star. The central part of the cross-correlation function consists of two components: a broad baseline, due to residuals in the continuum subtraction and blended features in the spectrum, on which a narrow and well defined peak is superposed. Because of the more accurate fit to the continuum performed here, the relative amplitude of the baseline with respect to the central peak is much smaller than in Dalle Ore et al. (1991; see their Fig. 4), being only about 10%–15% of the total signal. We fitted the wings of the baseline using a second-degree polynomial and subtracted it from the cross-correlation function.

The central peak was then fitted with a Gaussian, whose center gives the radial velocity of the galaxy with respect to the template star; its width (i.e., the FWHM), after subtracting in quadrature the width of the autocorrelation function (the template spectrum cross-correlated with itself), provides the width of the broadening function, i.e., the velocity dispersion.

Only the region of the spectrum blueward of $\lambda \simeq 6500$ Å has been used, in order to prevent contamination of the correlation function by the emission lines. Residuals from strong sky lines were masked out.

In order to estimate the uncertainties on the stellar kinematical measurements, rather than rely on the formal errors provided by the cross-correlation technique, we have followed a more empirical approach based on the assumption of perfect symmetry between the two sides of each spectrum. This assumption is justified by the high degree of symmetry shown by the stellar velocity and sigma profiles, even in those objects with kinematical peculiarities.

For each galaxy, we computed the differences in velocity (or more precisely, its absolute value) ΔV and in velocity dispersion $\Delta \sigma$ between points located symmetrically with respect to the kinematical center and associated them to the local line strength (i.e., the average signal in the absorption lines), L_S. The data for all spectra have been merged together, and a smooth curve was then interpolated through the data points in the $L_S - \Delta V$ and $L_S - \Delta \sigma$ plots. This curve was then used to compute the error bars for the data points in each galaxy spectrum. We notice that this method cannot be applied to emission lines, since the gaseous kinematics often exhibits marked deviations from regular and symmetric behavior.

Different cross-correlation runs were performed on each spectrum, using different spatial bins. The results were then combined, so as to maximize the spatial resolution in the central regions while smoothing out the noise in the external parts.

We have compared the velocity dispersions obtained for each object using different template stars or varying within reasonable limits the parameters in the cross-correlation algorithm; they all agree within $\pm 5\%$, in line with what is reported in the literature. Final rotation curves and velocity dispersion profiles were then obtained by averaging the measurements from the different templates, after bringing them into a common reference system by correcting for the radial velocity (computed with respect to an appropriate synthetic rest-frame spectrum) of each template.

We determined the stellar kinematical centers for each spectrum by finding the point about which the folded rotation and dispersion curves show the maximum kinematical symmetry. They generally agree with the photometric center to within ± 2 pixel (1″.2).

5. RESULTS

Stellar and gas rotation curves and stellar velocity dispersion profiles are presented in Figure 2.[2] They terminate at the radial distance where the differences between the two sides become larger than the error bars, or when we judge that the error bars are too large for the measurement to be of any use.

In a few cases, the radial extension on one side is smaller than on the other, because of the presence of a foreground star or a companion galaxy falling on the slit.

Table 2 lists the main kinematical parameters for the galaxies studied. Maximum rotation velocities and corresponding radii for the gas are given only for those galaxies with regular and symmetrical rotation curves.

In what follows we discuss the main kinematical characteristics and peculiarities of each galaxy in our sample.

NGC 3379.—This nearby galaxy shows gas emission concentrated in a small nuclear region. We were able to model the stellar continuum using the signal outside the line-emitting region (at $r > 10''$) and subtract it from the central spectral rows. We then measured the position of the [N II] and Hα lines on the resulting continuum-free spectrum; reliable data were obtained only in the central 5″. A detailed analysis of the kinematic properties of this galaxy is presented in Pastoriza et al. (2000).

NGC 3489.—In this lenticular, gas and stars show fast rotation along the major axis (P.A. = 76°) of the gas distribution, which roughly coincides with the major axis of the stellar isophotes. The gas also shows rotation along the minor axis, though with a somewhat irregular behavior; no stellar rotation is seen. There is evidence for a distinct nuclear stellar component ($r \simeq 3''$): it is visible on the major axis as the central part of the rotation curve delimited by the sharp discontinuities in its slope, and on the minor axis as a small rotating core.

NGC 3607.—For this S0 galaxy, we only have data along the major axis (which is also the major axis of the gas distribution). The gas rotation curve, which has a steeper gradient than the stellar one, reaches its maximum at $r \simeq 7''$ and then stays flat out to the last observed point ($r \simeq 16''$). The stellar rotation curve presents a maximum at $r \simeq 5''$ and then decreases steadily; the stellar velocity dispersion exhibits a central peak, then decreases slowly to $\sigma \simeq 200$ km s^{-1}.

NGC 4105.—This S0 was observed only along the major axis of the line-emitting region, a little skewed ($\simeq 5°$) with respect to the photometric major axis (P.A. = 151°; de Vaucouleurs et al. 1991, hereafter RC3). The gas rotates much faster and in the opposite direction to the stars and presents a somewhat different behavior on the two sides: the NW part shows a less steep central gradient, and a dip at about 13″.

NGC 4472.—We obtained a continuum-free spectrum of the central part in the same way as we did for NGC 3379.

NGC 3379   PA=70

NGC 3379   PA=115
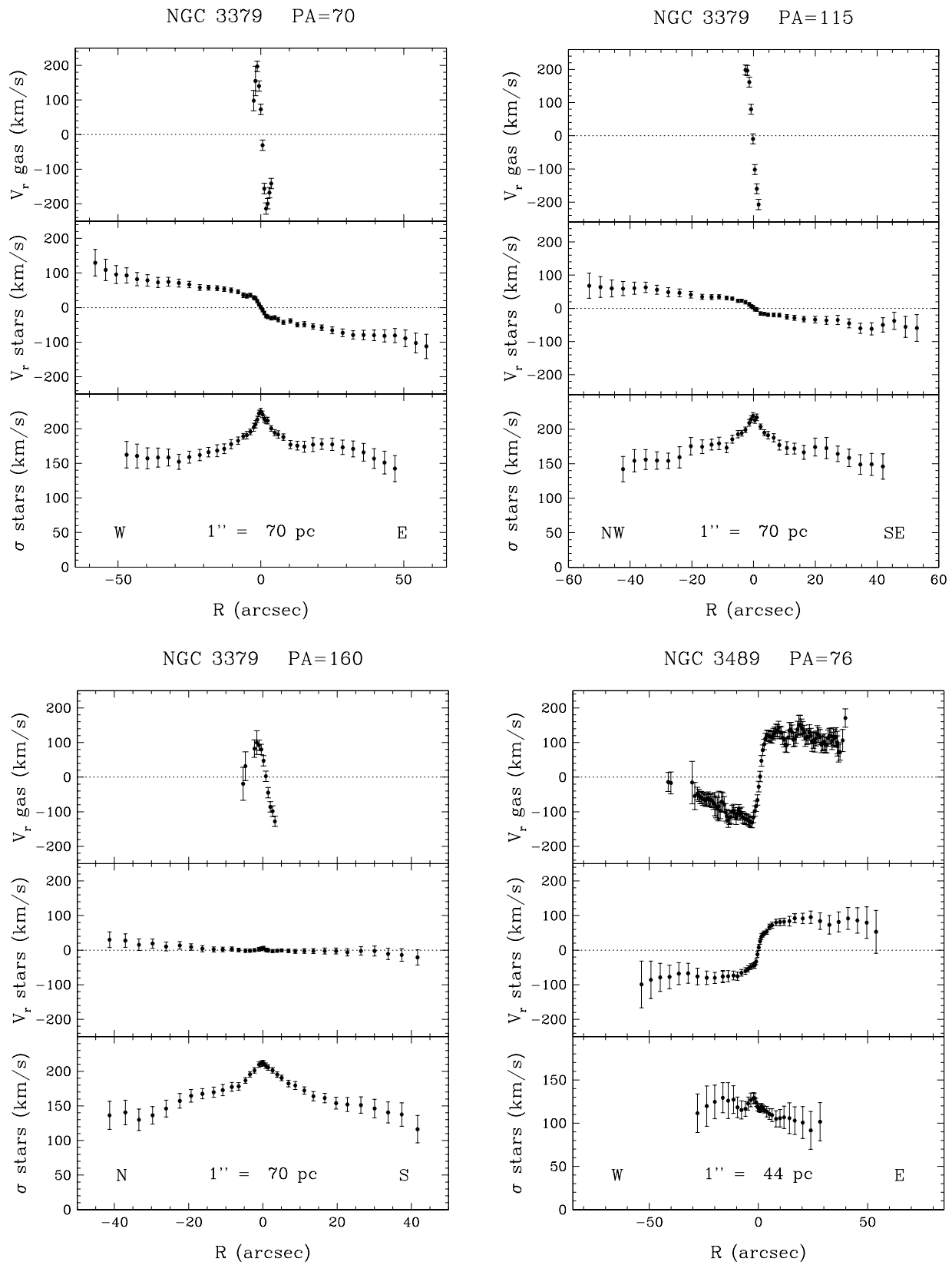
NGC 3379   PA=160

NGC 3489   PA=76

Fig. 2.—Gas and stars kinematics. (*Top*) Velocity profile of the gas; (*middle*) stellar rotation curve; (*bottom*) stellar velocity dispersion profile.
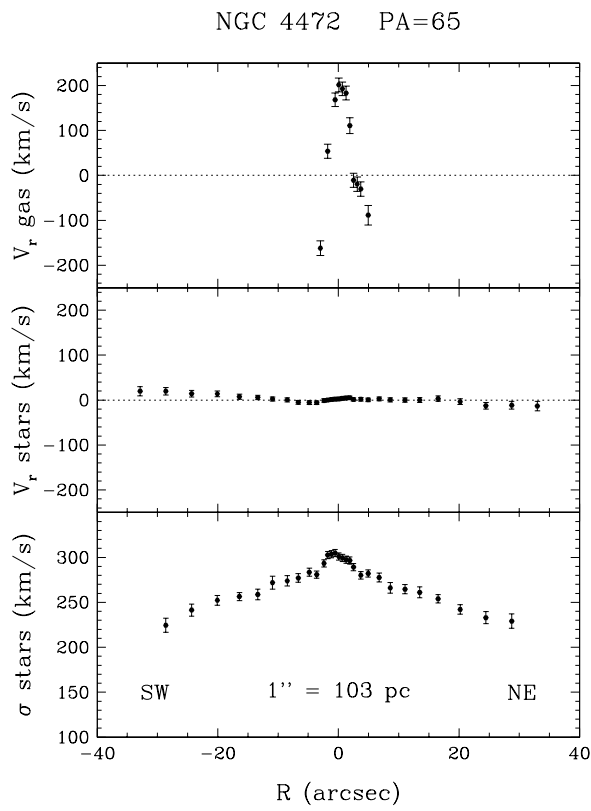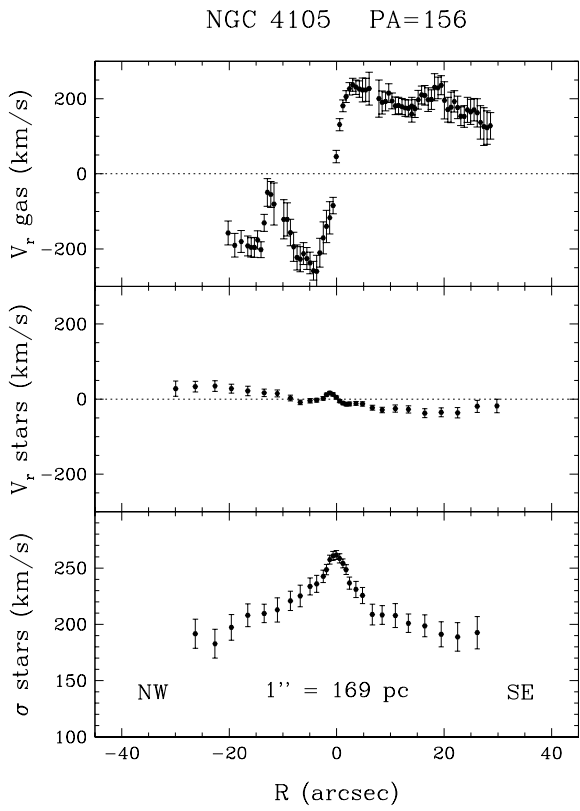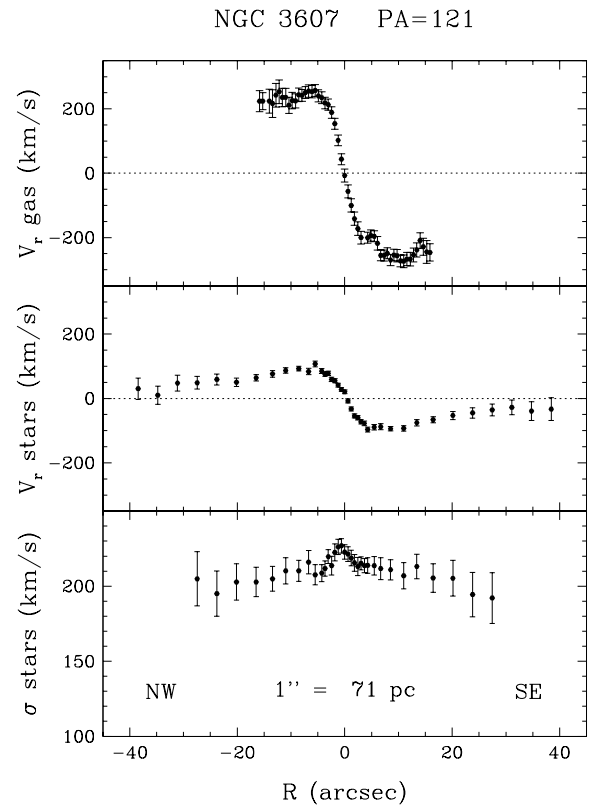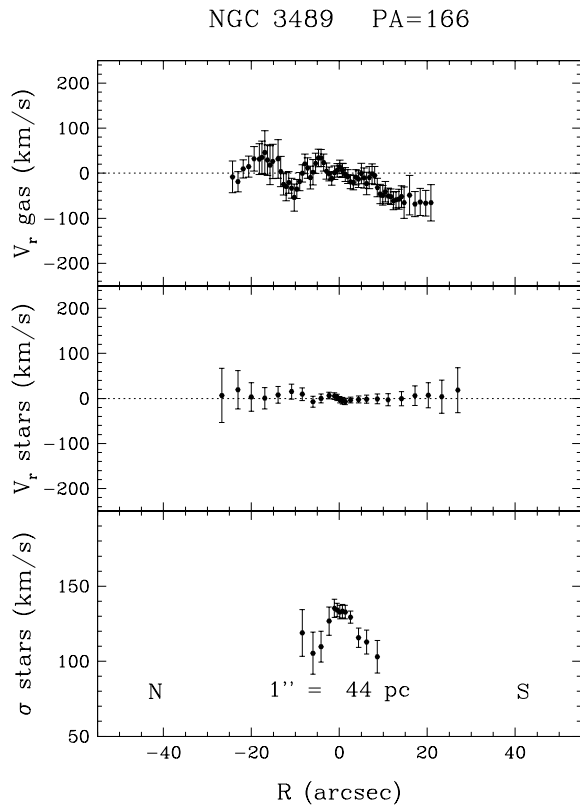
NGC 3489   PA=166

NGC 3607   PA=121

NGC 4105   PA=156

NGC 4472   PA=65

FIG. 2.—*Continued*

47

NGC 4472   PA=155

NGC 4636   PA=27

NGC 4636   PA=117

NGC 4636   PA=141

FIG. 2.—*Continued*

48

NGC 5044   PA=10

NGC 5044   PA=40

NGC 5044   PA=90

NGC 5077   PA=10

FIG. 2.—*Continued*

NGC 5077   PA=108

NGC 5813   PA=43

NGC 5813   PA=99

NGC 5846   PA=180

Fig. 2.—Continued

50

NGC 5898   PA=62

NGC 5898   PA=152

NGC 5903   PA=160

NGC 6758   PA=63

Fig. 2.—*Continued*

NGC 6758   PA=153

NGC 6868   PA=30

NGC 6868   PA=70

NGC 6868   PA=120
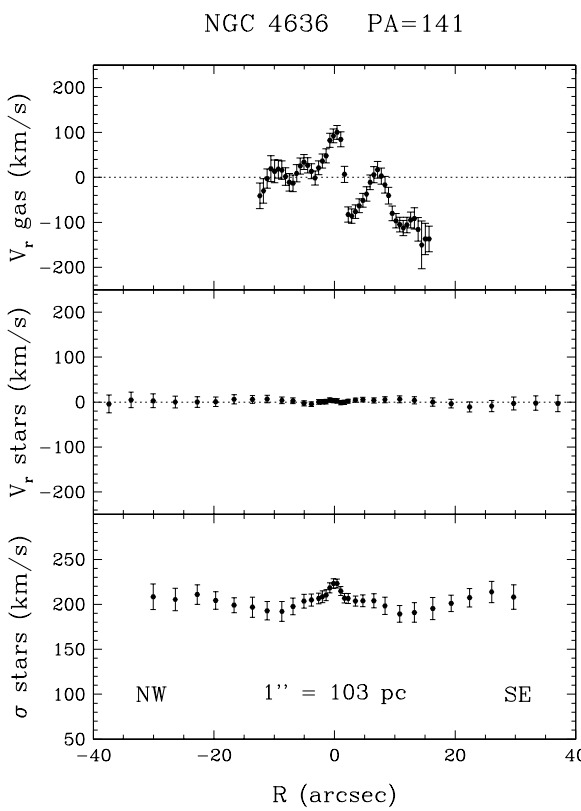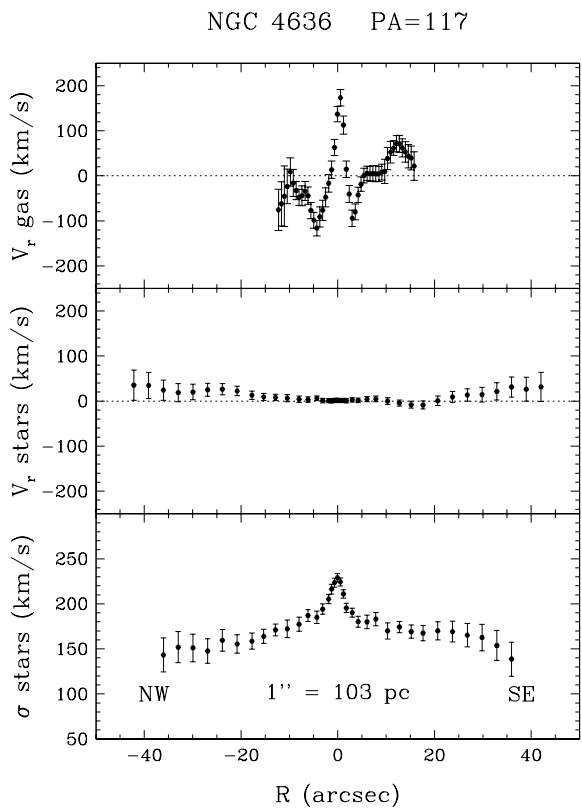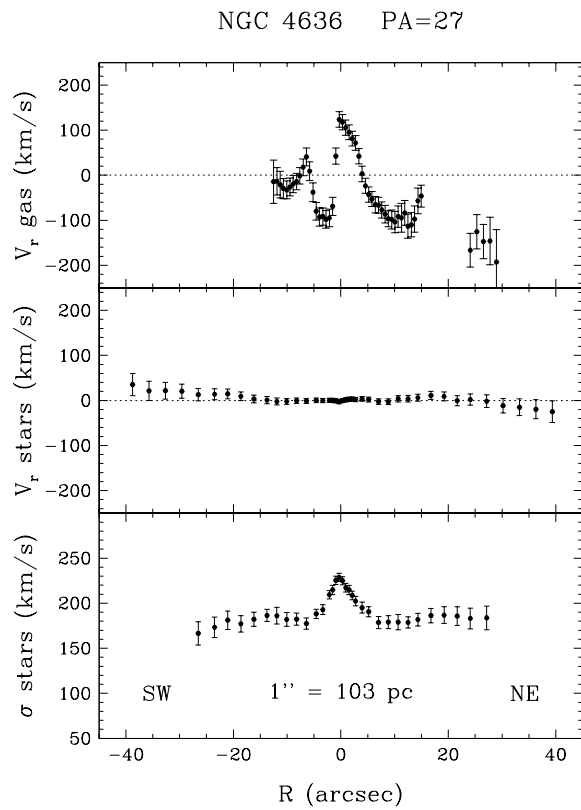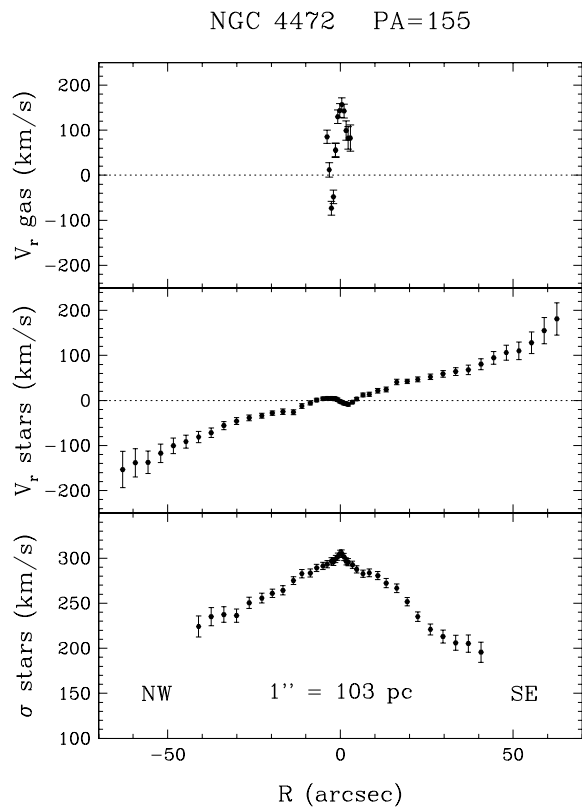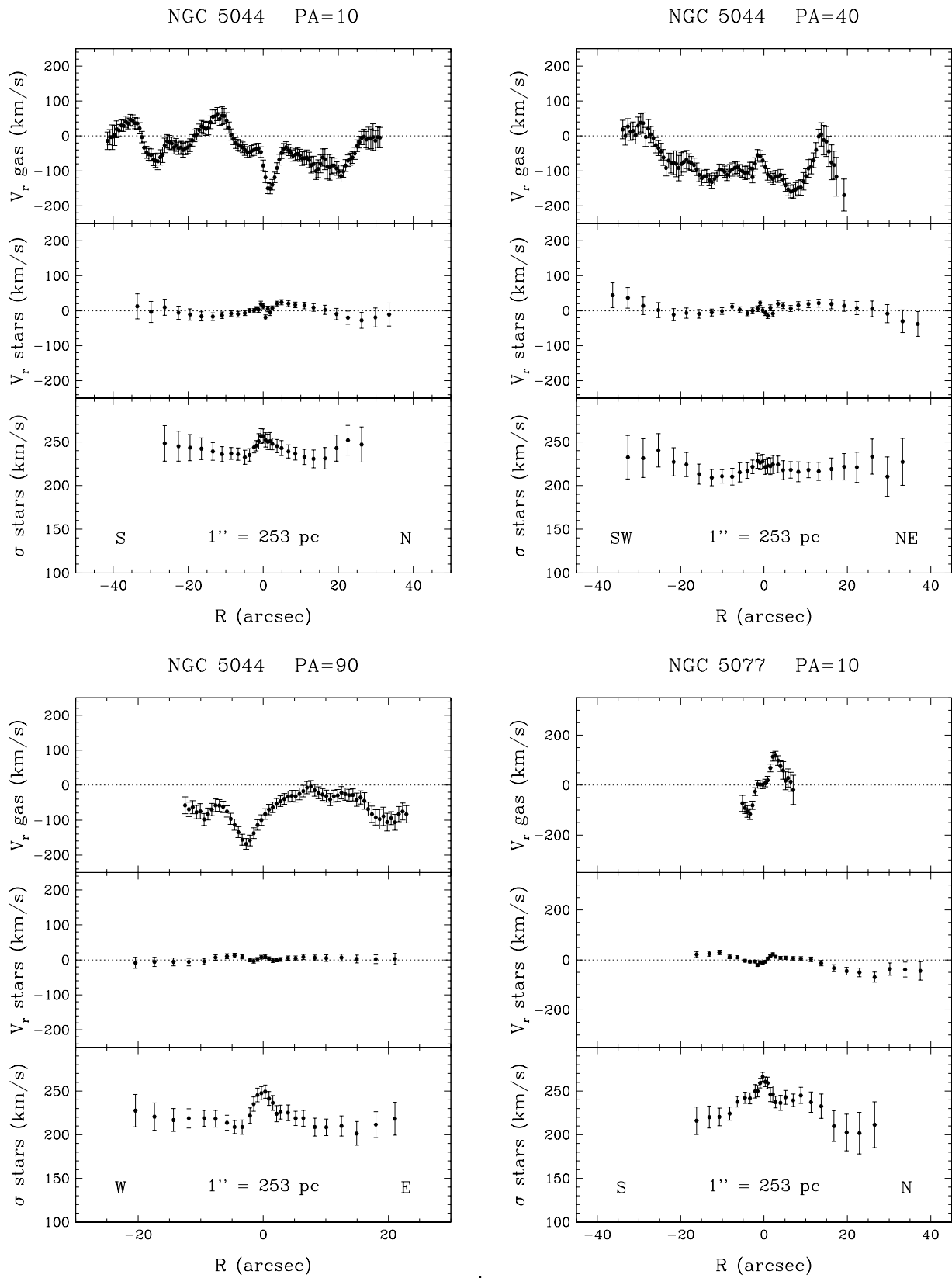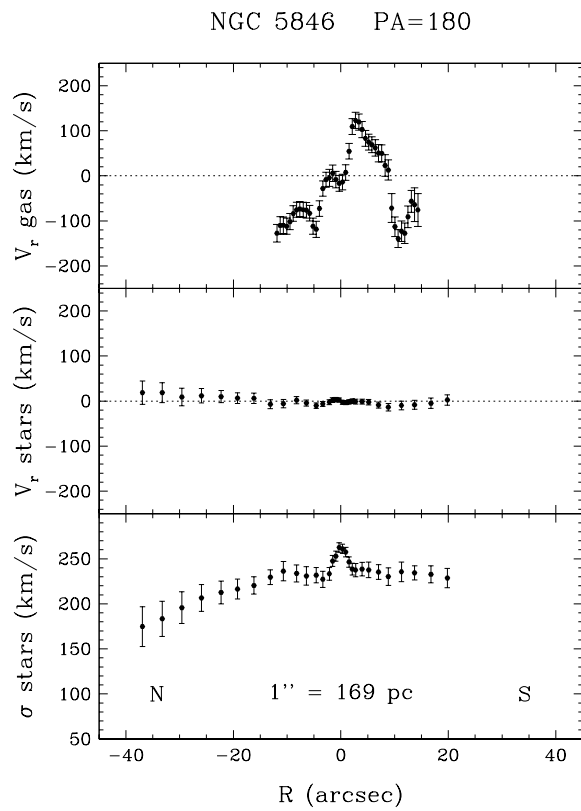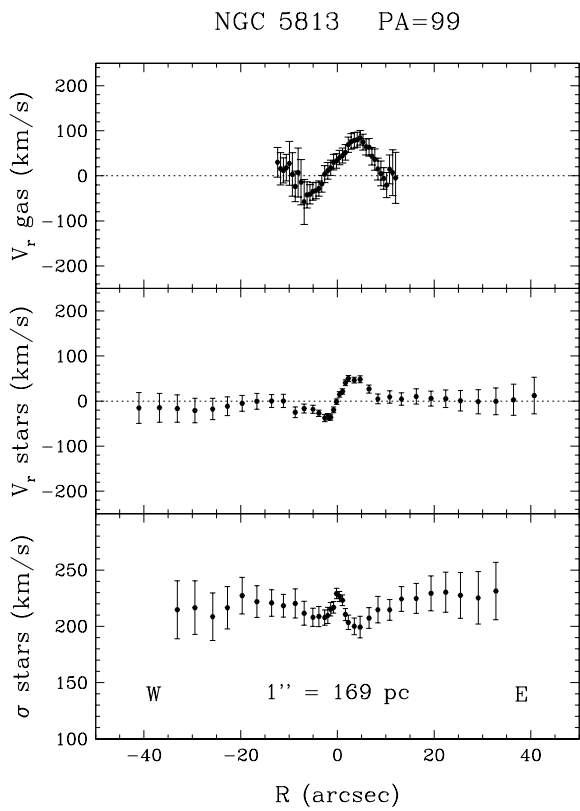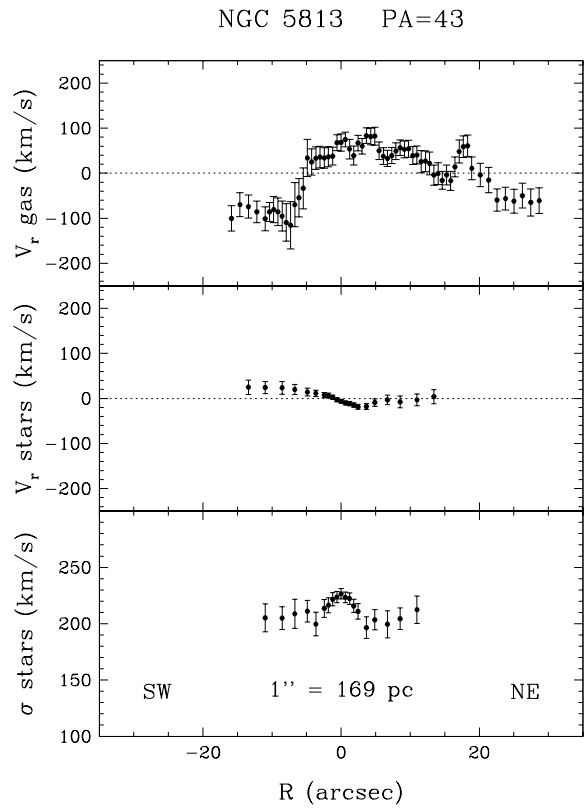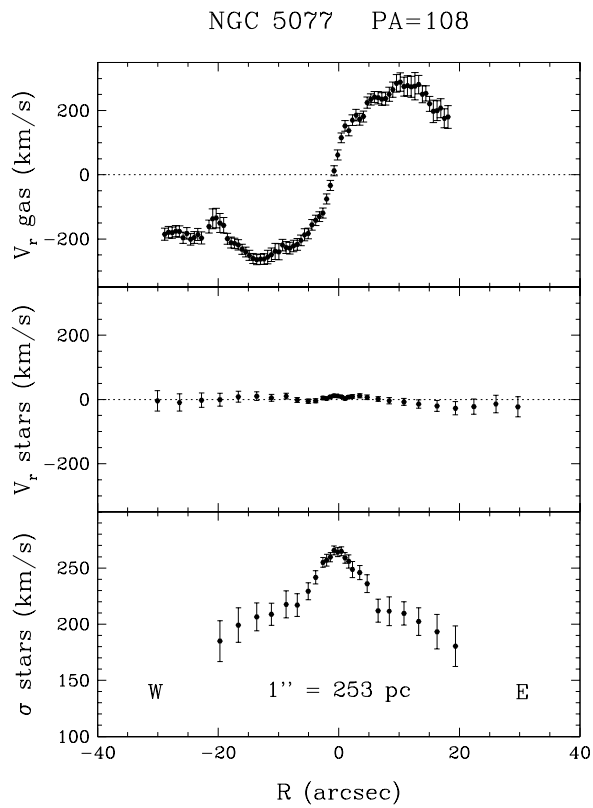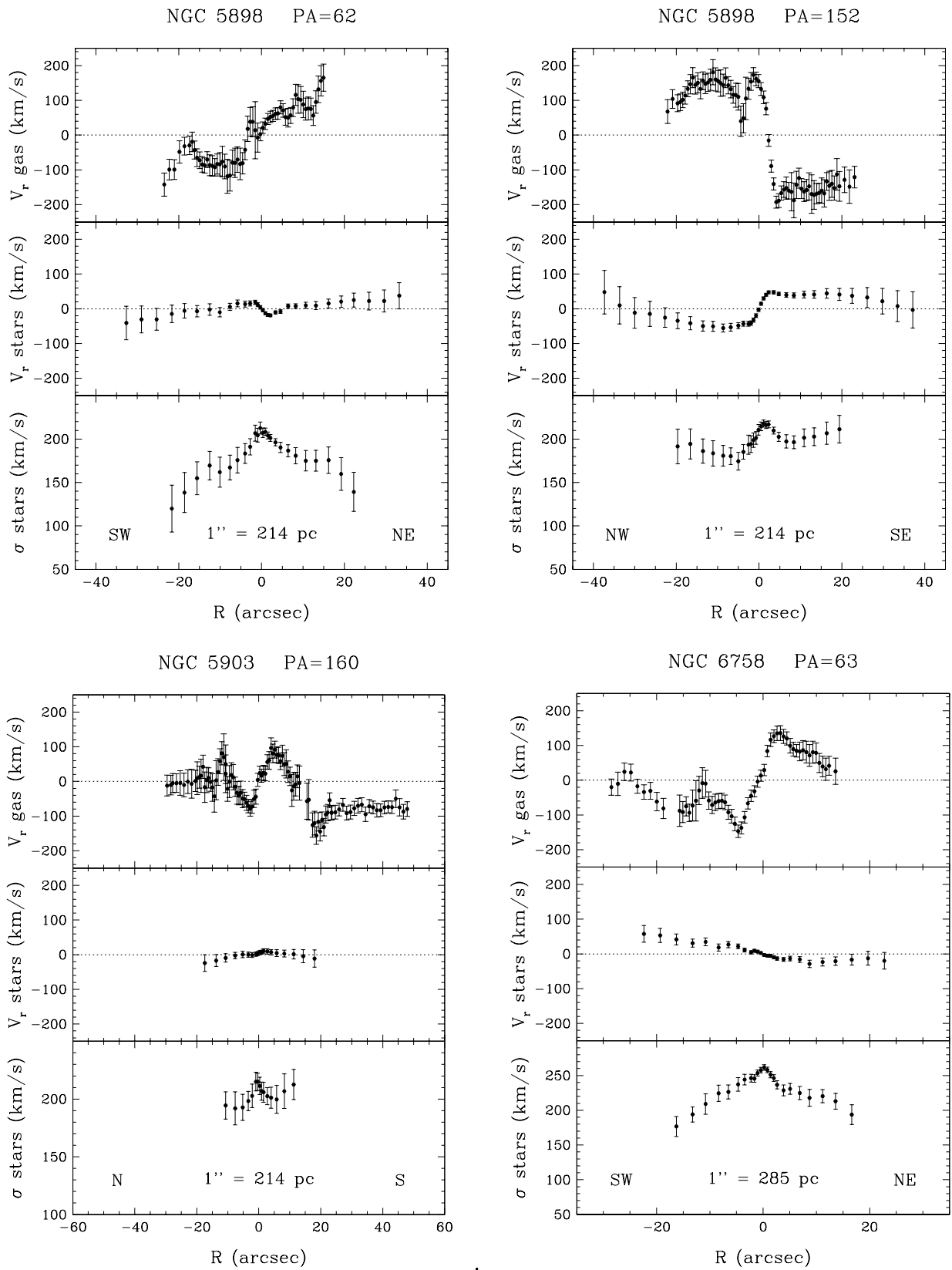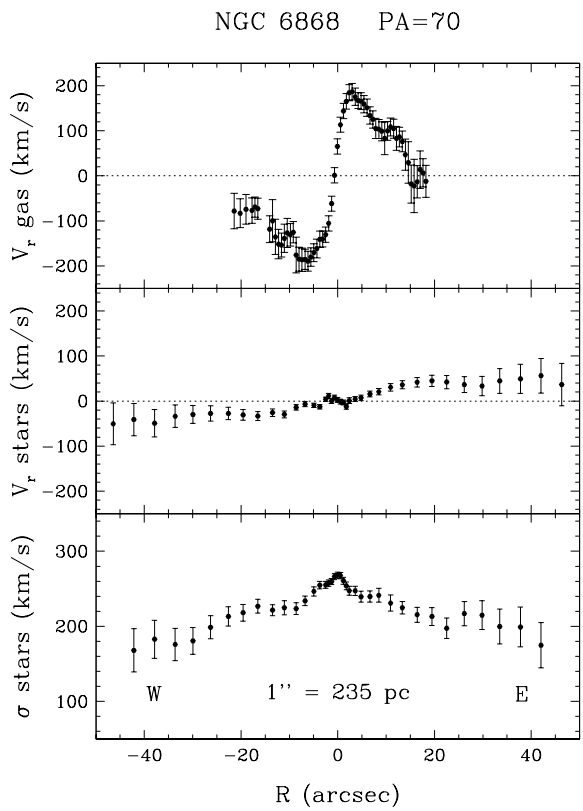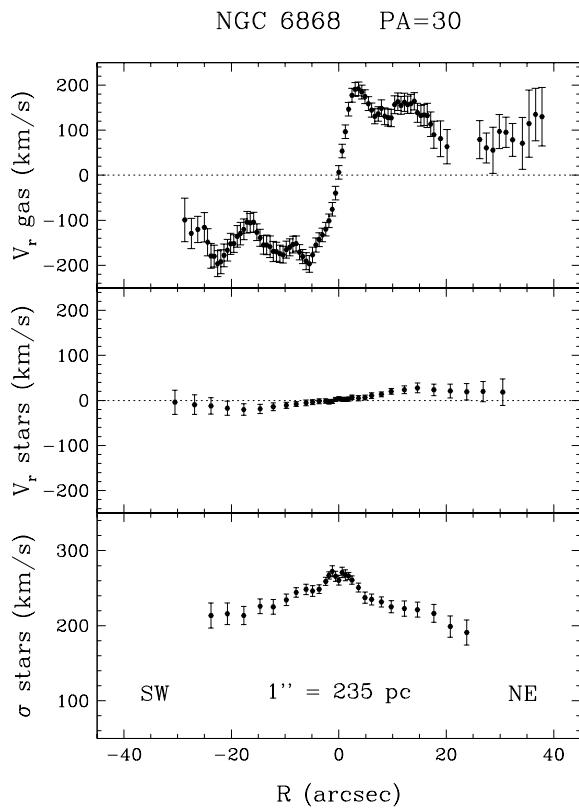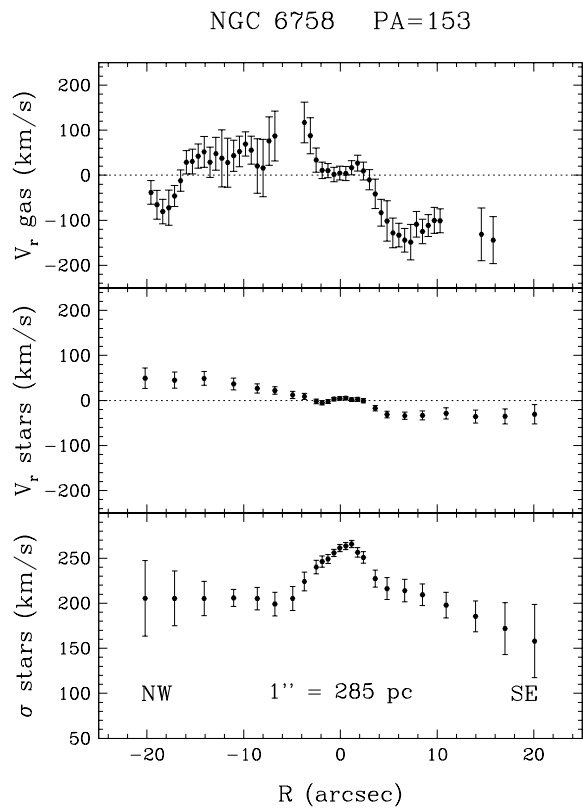
FIG. 2.—*Continued*

TABLE 2

MAIN KINEMATICAL PARAMETERS
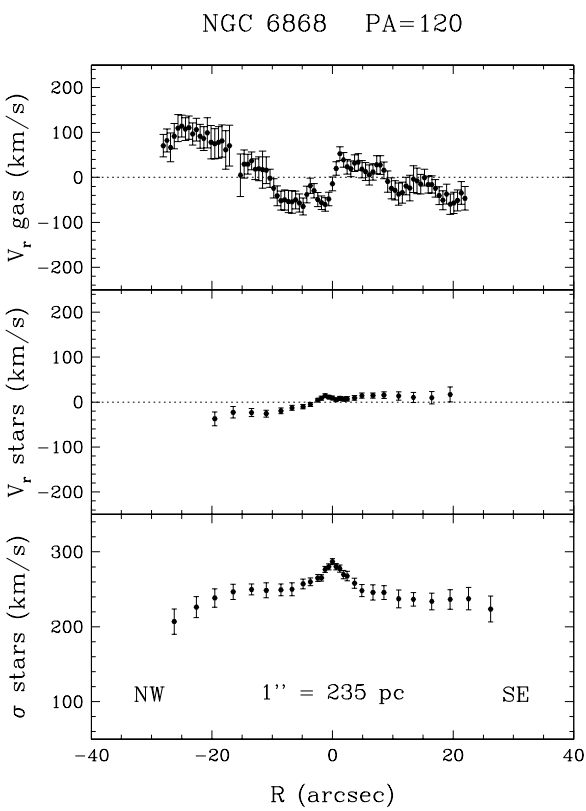
Identification	P.A. (deg)	σ_c (km s^{-1})	V_{max} (km s^{-1})	R_{max} (arcsec)	V_{max}(gas) (km s^{-1})	R_{max}(gas) (arcsec)
NGC 3379......	70	223 ± 6	105 ± 20	55R	210 ± 20	2
	115	216 ± 5	50 ± 10	45	210 ± 20	2
	160	212 ± 4	22 ± 6	42R	100 ± 30	2
NGC 3489......	76	117 ± 4	87 ± 5	24	130 ± 15	8
	166	133 ± 5	13 ± 10	23	Irr.	...
NGC 3607......	121	223 ± 5	100 ± 8	6	250 ± 30	11
NGC 4105......	156	261 ± 4	36 ± 7	21	240 ± 20	4
NGC 4472......	65	305 ± 4	17 ± 8	33	Irr.	...
	155	302 ± 4	115 ± 10	45R	Irr.	...
NGC 4636......	27	226 ± 5	25 ± 15	38R	Irr.	...
	117	229 ± 5	...	...	Irr.	...
	141	223 ± 5	6 ± 11	25	Irr.	...
NGC 5044......	10	256 ± 8	14 ± 12	15	Irr.	...
	40	225 ± 8	40 ± 20	37R	Irr.	...
	90	248 ± 8	5 ± 12	20	Irr.	...
NGC 5077......	10	262 ± 5	50 ± 20	25	115 ± 10	3
	108	264 ± 4	12 ± 20	20	270 ± 10	13
NGC 5813......	43	225 ± 5	15 ± 8	3	Irr.	...
	99	231 ± 5	50 ± 8	3	Irr.	...
NGC 5846......	180	261 ± 5	10 ± 8	26	Irr.	...
NGC 5898......	62	213 ± 5	40 ± 20	33R	110 ± 25	8
	152	210 ± 5	47 ± 12	9	160 ± 20	13
NGC 5903......	160	212 ± 8	12 ± 20	18	Irr.	...
NGC 6758......	63	261 ± 4	40 ± 20	22	135 ± 15	4
	153	262 ± 4	40 ± 20	20	130 ± 15	7
NGC 6868......	70	267 ± 4	45 ± 25	42	180 ± 20	5
	30	266 ± 4	23 ± 10	15	190 ± 10	5
	120	284 ± 4	20 ± 8	11	Irr.	...

NOTES.—σ_c is the stellar central velocity dispersion, averaged within the central 3 pixels (1″8); V_{max} is the maximum rotation velocity, reached at radius R_{max} (an " R " next to R_{max} indicates that the velocity curve is still rising); V_{max}(gas) is the maximum rotation velocity of the gas, reached at R_{max}(gas). " Irr." means irregular velocity profile.

The well-known counter-rotating stellar core is evident in both axes. The gas rotation curves appear irregular; however, they may be influenced by the uncertainties on matching and subtracting the continuum from the observed spectrum.

NGC 4636.—The gas presents very irregular velocity curves, on all the three axes we observed; particularly interesting is the narrow velocity peak observed at P.A. = 117°. The photometric major axis is P.A. $\simeq$ 150° (RC3). As already noted by Zeilinger et al. (1996), turbulent motions or material not yet settled may be responsible for this behavior; unfortunately, our lack of the velocity dispersion profiles for the gas prevents us from confirming this interpretation. The stellar velocity curve at P.A. = 27° shows a central nonrotating region, with radius of about 0.5 kpc, corresponding to the peak in the sigma profile; then the rotation velocity increases slowly out to the last observed point. No stellar rotation is visible at P.A. = 141°. We cannot explain the rather odd velocity curve at P.A. = 117°; the dispersion profile seems regular, though.

NGC 5044.—This is a very peculiar object. The gas velocity profile is very irregular, with many humps and dips; its radial velocity is systematically blueshifted with respect to the stellar systemic velocity by $\sim$60–100 km^{-1}. Furthermore, the stellar velocity curves at P.A. = 40° and P.A. = 10° show a fairly large central part of the galaxy, with radius $\simeq$25″ (about 6 kpc, 1/3 of the effective radius), counter-rotating with respect to the outer regions; very

slow or no stellar rotation is visible along the galaxy minor axis (P.A. = 90°). There are evident irregularities in the very center of all three stellar rotation curves, although their small size and amplitude make it unclear whether they represent a real distinct kinematical subcomponent. The velocity dispersion of the gas peaks at $\sim$200–230 km s^{-1} in the center and decreases rapidly outward. Secondary peaks, of smaller amplitude ($<$160 km s^{-1}) may be present, especially along P.A. = 10°.

NGC 5077.—This galaxy, classified as S0, exhibits a gaseous disk with major axis roughly orthogonal to the galaxy photometric major axis (P.A. $\simeq$ 10°). However, the gas isophotes appear to change position angle at increasing radial distances, starting from the very center. A marked warp is visible on the W side at $R \simeq$ 20″. The gas presents a fairly symmetric and smooth rotation curve at P.A. = 108°, reaching maximum velocity ($\simeq$270 km s^{-1}) at $r \simeq$ 13″. Along this axis, stars show very slow rotation. At P.A. = 10°, the stellar rotation curve exhibits a counter-rotating core ($r \leq$ 5″, 1.2 kpc), corresponding to a marked central peak in the velocity dispersion profile (the profiles are terminated at $r \simeq$ 17″ on the W side due to a star falling on the slit). On this same axis, the gas rotates in the same direction as the stellar nucleus and shows a tiny central plateau. This galaxy has been thoroughly studied and modeled by Bertola et al. (1991); due to their larger error bars, they do not recognize the counter-rotating core (see their Fig. 1).

NGC 5813.—The stellar rotation curve at P.A. = 99° shows the kinematically decoupled stellar core discovered by Efstathiou, Ellis, & Carter (1982), and further studied by Kormendy (1984). There is excellent agreement between our data and theirs (compare with Fig. 1 in the former paper): we observe the central peak in the velocity dispersion curve, the minimum at $r \simeq 3''$, and then the rise out to $r \sim 20''$. Our data do not extend far enough to see the decrease at larger radii. We measure $V_{max} = 50 \pm 8$ km s^{-1}, compatible with their value of 89 ± 7 km s^{-1}, taking into account the 31° difference in the slit angle.

Slow rotation is also seen along P.A. = 43°. The gaseous velocity profiles on both position angles are irregular and may be the result of still unsettled material, which shows up as a filamentary structure in the Hα + [N II] map. The gas velocity dispersion peaks at about 200 km s^{-1} in the galaxy center.

NGC 5846.—We only observed one position angle, P.A. = 0°. The stars show slow rotation, if any; the profile is cut at $r \simeq 25''$ on the S side due to a companion galaxy falling on the slit. The gas displays an irregular velocity profile, with a central plateau, a very steep gradient on both sides, and then a rapid change in velocity direction on the S side.

NGC 5898.—A counter-rotating core is observed on the galaxy major axis (P.A. = 62°), with transition radius $\simeq 5''$ (1 kpc); the rotation curve of the main spheroid keeps rising out to the last observed point. Along this same axis, the gas rotates in the same sense as the stellar body, although not in a smooth fashion and presents a "hump" a few arcsec offset to the SW. The minor axis, P.A. = 152°, shows the gas rotating in a sense opposite to the stars, with its barycenter possibly displaced by a couple of arcsec SE, in line with the asymmetric distribution of the ionized gas visible in the Hα + [N II] map; also, there is a velocity dip at $r \simeq 5''$ on the NW side. This galaxy was studied by Bertola & Bettoni (1988); as their data points at P.A. = 60° only extend out to $\sim 10''$, they fail to recognize the change of rotation sense outside the central region.

NGC 5903.—There is faint, diffuse emission visible and measurable in our spectrum out to $r \simeq 50''$ along the S side, which is not visible in our Hα + [N II] map as it was below our detection threshold. Stars show little rotation, while the gas presents an irregular velocity profile.

NGC 6758.—We see an overall regular gaseous rotation curve at P.A. = 63°, reaching maximum amplitude ($\simeq 140$ km s^{-1}) at $\simeq 4''$ (0.8 kpc) and then decreasing to $V_R \sim 0$. The stars rotate in a sense opposite to the gas, and more slowly ($V_{max} \simeq 40$ km s^{-1}). The gas velocity curve at P.A. = 153° is more irregular, though it shows a definite rotation sense coincident with that of the stars. The central plateau ($r < 3''$) visible in the stellar velocity curve suggests the presence of a nuclear region with an angular momentum vector misaligned with respect to that of the main body.

NGC 6868.—The gas exhibits a more or less regular rotation curve at P.A. = 30° and P.A. = 70°, in agreement with the stellar rotation; at P.A. = 120°, the gas counter-rotates with respect to stars, and it even shows a sort of inner counter-rotating component, somewhat offset to the NW side with respect to the kinematical center for the stars. Zeilinger et al. (1996) already noticed this feature and explain it as the superposition of two unresolved components rotating in a sense opposite to each other, one dominating in the inner region, the other dominating in the

external parts. The present spectral resolution does not allow us to check their conclusions.

The central velocity dispersion of the gas is $\simeq 170$ km s^{-1}. A kinematically decoupled, counter-rotating core is visible in all three stellar velocity curves, more evident at P.A. = 70°, where the kinematical break radius is $r = 3''$ (0.7 kpc); at P.A. = 30°, the velocity dispersion appears to fall toward the very center.

6. COMPARISON WITH THE LITERATURE

In order to assess the quality of our data and to check for the presence of possible systematic effects related to the instrumental resolution we used, we have compared our rotation curves and velocity dispersion profiles with published measurements. This comparison also permits a more general valuation of the typical uncertainties and degree of (dis)agreement among different authors, with evident implications on the accuracy and reliability of those galaxy models built on gaseous and stellar kinematics data.

For the stellar kinematics, we have used the tabulated values present in Hypercat (see Prugniel et al. 1998; http://www-obs.univ-lyon1.fr/hypercat/). We limit ourselves to show comparisons for the two most popular galaxies in our sample, i.e., NGC 3379 (Figs. 3 and 4) and NGC 4472 (Figs. 5 and 6). For NGC 4472, we collected data from Davies & Birkinshaw (1988, hereafter DB); Franx, Illingworth, & Heckman (1989, hereafter FIH); Bender, Saglia, & Gerhard (1994, hereafter BSG); Fisher, Illingworth, & Franx (1995). For NGC 3379, we use data from DB, FIH, BSG, and from Statler & Smecker-Hane (1999, hereafter SS). Our kinematics show generally good agreement with the literature, with the possible exception of the velocity dispersion profiles of NGC 4472 at P.A. = 155°, where our data seem to
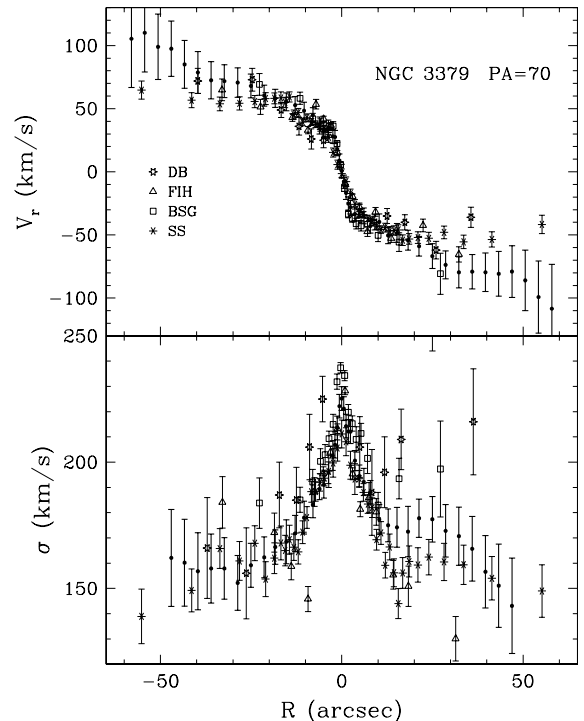

Fig. 3.—Comparison with the literature for NGC 3379, at P.A. = 70° (major axis). The thick error bars show our measurements. Our rotation curve keeps increasing at $r > 30''$, while in SS it flattens off at that radius.
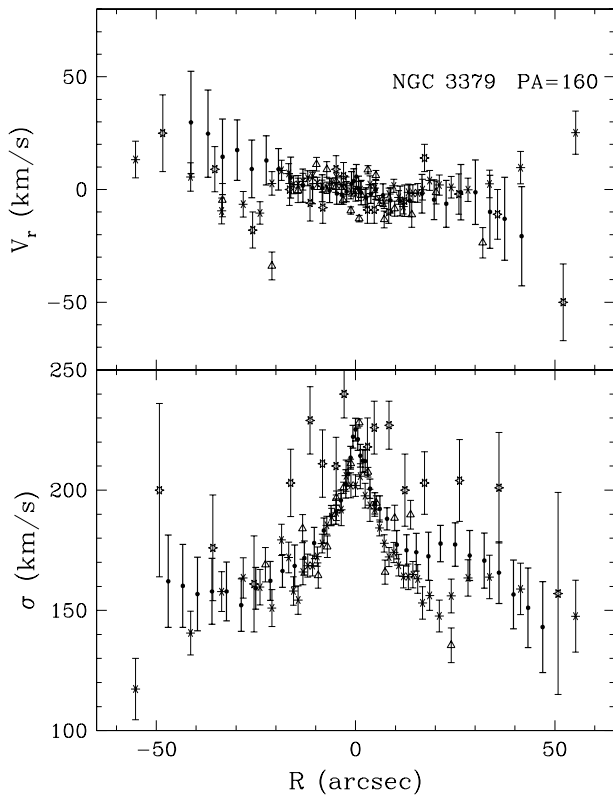
FIG. 4.—Comparison with the literature for NGC 3379, at P.A. = 160° (minor axis). Notice the large scatter among measurements from different authors.
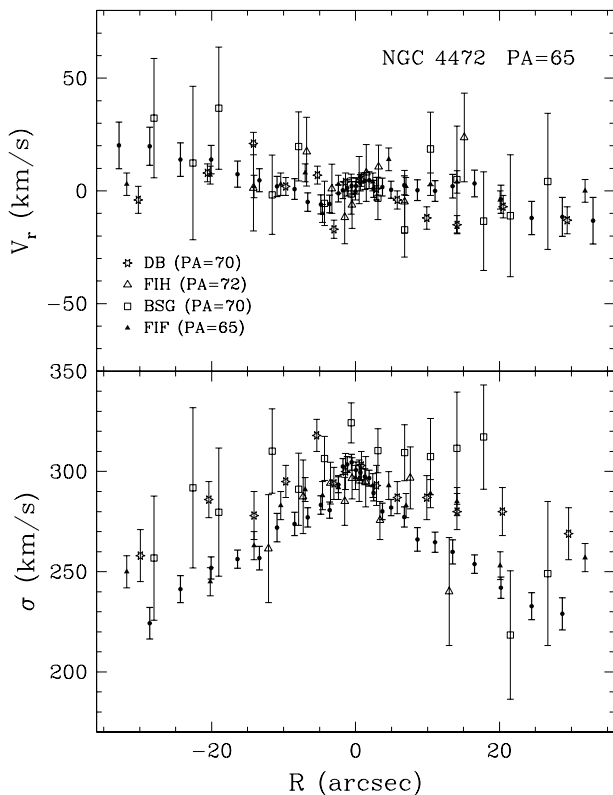

FIG. 5.—Comparison with the literature for NGC 4472, along the minor axis at P.A. = 65° (for DB and BSG: P.A. = 70°; for FIH: P.A. = 72°).
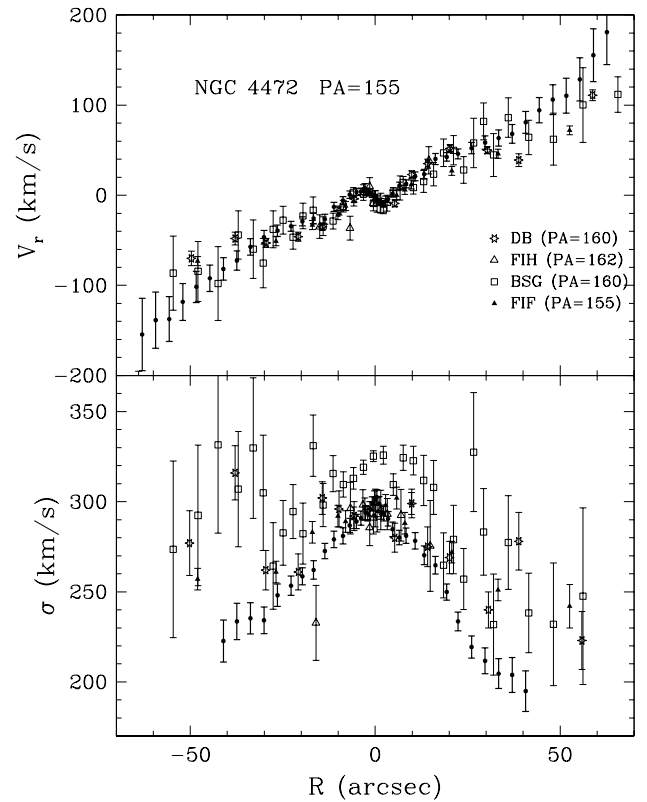

FIG. 6.—Comparison with the literature for NGC 4472, along the major axis at P.A. = 155° (for DB and BSG: P.A. = 160°; for FIH: P.A. = 162°). Notice that the asymmetry visible in our dispersion profile (the SE side decreases faster than the NW side) is also present, though less clear, in the literature data. Also, our rotation curve shows a steeper gradient in the outer regions.

show a more rapid decrease of σ. However, we notice that there is quite a large scatter among the different data sets, especially in the σ measurements; differences as large as 50–100 km s^{-1} are present even at small galactocentric distances.

Gaseous and stellar kinematics for NGC 5077 have been studied by Bertola et al. (1991); comparisons are presented in Figures 7 and 8. There is broad agreement for the data at P.A. = 108°, taking into account the ~10° offset in position angle. Less satisfactory is the comparison at P.A. = 10°, where the rotation curves of the ionized gas differ significantly; in particular, we see a rapidly rising rotation velocity within ±3″, whereas Bertola et al.'s curve shows a more uniform and smooth profile. A poorer spatial resolution in the earlier data could explain the discrepancy.

Zeilinger et al. (1996) present gas kinematics for two objects in our sample, NGC 4636 and NGC 6868; they are plotted with our data in Figures 9 and 10. In NGC 6868, there is excellent agreement among the two data sets at P.A. = 30° and P.A. = 70°, while the curves at P.A. = 120° show a discrepancy in the central 5″. For NGC 4636, the agreement is good at P.A. = 28° and P.A. = 148°, while there is significant disagreement at P.A. = 118°. A possible explanation may be slightly different positionings of the slit.

Finally, we have compared our values for the stellar central velocity dispersion with the averaged values published in Hypercat. Figure 11 shows a good match between the two sets of data, with no systematic offsets or trends. The mean difference is −1.6 km s^{-1}, with a rms of
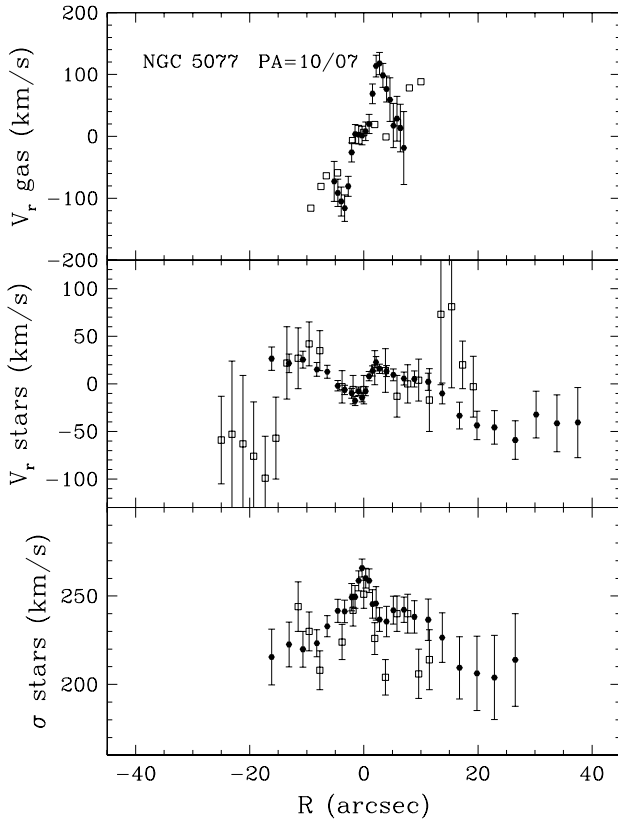
FIG. 7.—Comparison of our NGC 5077, P.A. = 10° kinematics (major axis of the stellar component; *filled circles*) with data from Bertola et al. (1991) at P.A. = 07° (*empty squares*).
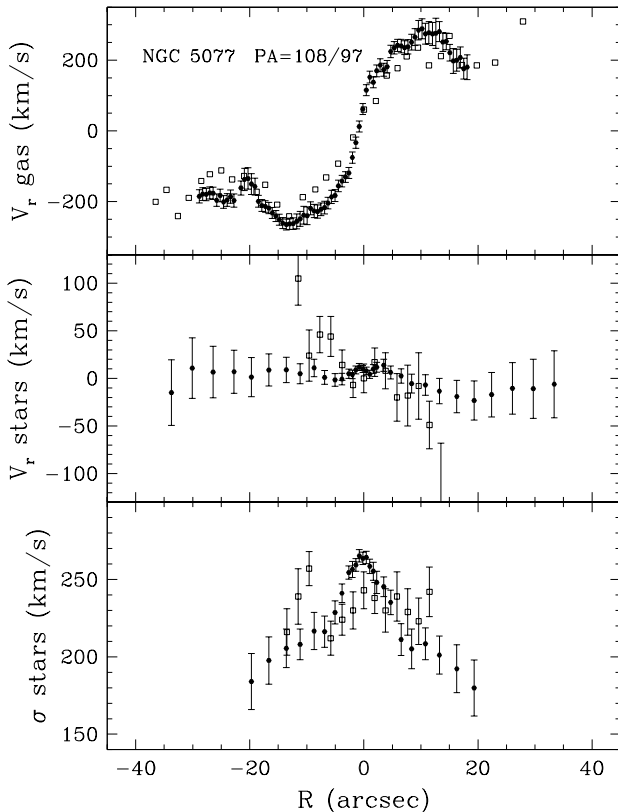

FIG. 8.—Comparison of our NGC 5077, P.A. = 108° kinematics (∼major axis of the ionized gas distribution) with data from Bertola et al. (1991) at P.A. = 97°.
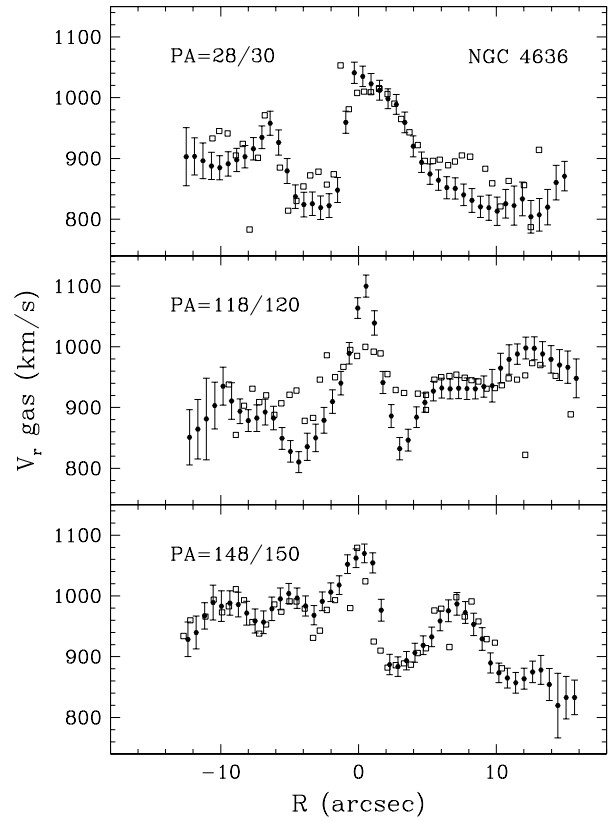

FIG. 9.—Comparison with Zeilinger et al. gas kinematics (*empty squares*) for NGC 4636. No error bars are available for their measurements. There is a 2° difference in the position angles. Zeilinger et al. data have been slightly shifted on both axes to allow for small difference in the spatial and velocity zero points.

7.7 km s^{-1}. Only NGC 3489 and NGC 4636 show differences larger than 12 km s^{-1}.

7. DISCUSSION AND CONCLUSIONS

The main kinematical characteristics of the galaxies in the present sample are summarized in Table 3.

The majority have irregular, sometimes chaotic gas kinematics; the five galaxies with overall regular gaseous rotation curves are all classified as S0.

NGC 4636 and NGC 5044 are the most striking example of the first group. Their gaseous velocity profiles show that the gas is not in a dynamical equilibrium status; NGC 5044 even displays a significant offset between the systemic velocities of gas and stars.

We detect gas/star counter-rotation in five galaxies, i.e., NGC 4105, NGC 5813, NGC 5898, NGC 6758, and NGC 6868. We notice that counter-rotation might be seen on one axis, while gas and stars appear to corotate on a different axis, as in NGC 5898. If the angular momentum vector of the ionized gas is misaligned with respect to that of the stellar body (but not antiparallel to it), the presence or not of counter-rotation depends on the particular view angle. Since we do not have a complete kinematical mapping of all of our objects (for some of them we only have one position angle), we might then fail to recognize other objects with misaligned gaseous and stellar kinematics.

We also find four, possibly five, galaxies (NGC 4472, NGC 5077, NGC 5898, NGC 6868 plus the less clear case of NGC 3489) that contain a counter-rotating stellar nucleus.
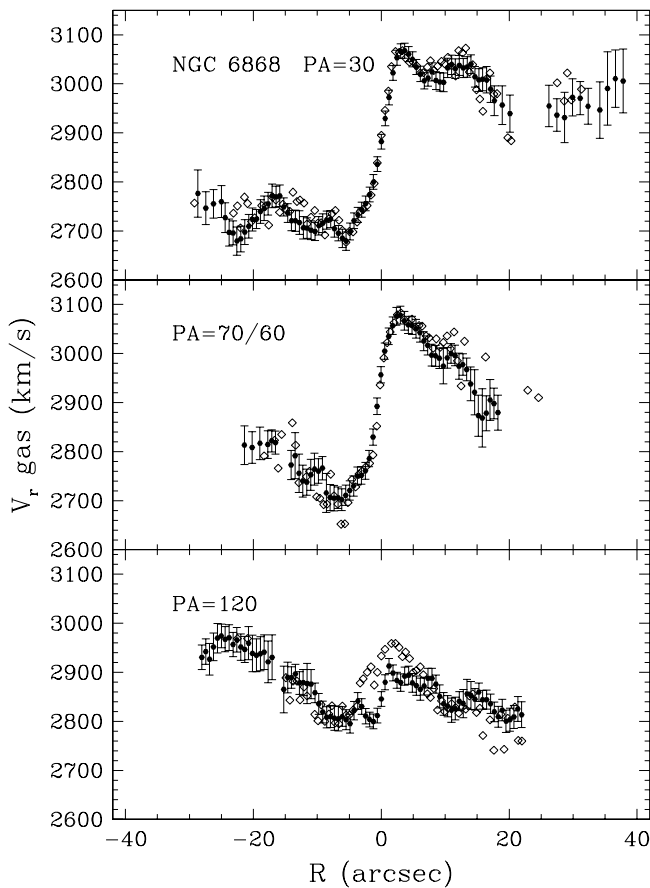
FIG. 10.—Comparison with the gaseous kinematics of Zeilinger et al. (*empty squares*) for NGC 6868. In the middle panel we plot our P.A. = 70° data and theirs at P.A. = 60°.
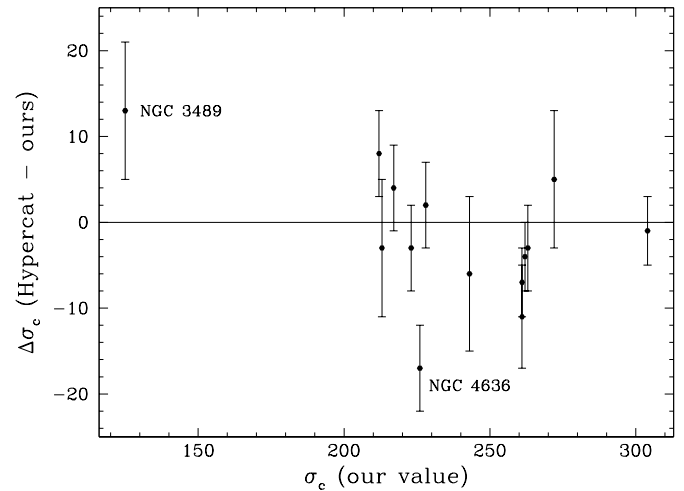

FIG. 11.—Differences between our central velocity dispersions (the averaged value is used when we have observed along different position angles) and the values reported in Hypercat.

In NGC 5044 there is a large inner region (size ≃ 10 kpc) that counter-rotates with respect to the outer parts, visible at P.A. = 10° and P.A. = 40°. This region itself probably contains a smaller, nuclear counter-rotating component. In NGC 4636 and NGC 6758 (and possibly in NGC 5846 too), though no star-star counter-rotation is detected, there is

evidence for the central region to be kinematically decoupled from the main stellar body, as shown by the marked change of slope in the central part of the velocity curve. Finally, NGC 5813 contains a fast rotating core, while the outer regions ($r > 1$ kpc) show a low rotation velocity ($V < 10$) km s^{-1}.

The percentage of galaxies with kinematically decoupled central regions in our sample appears to be quite large, ≃ 70%; unfortunately, there are no readily available statistics for cluster and field early-types in general. Therefore, we cannot determine whether gas-rich early-type galaxies do have a significantly enhanced proportion of peculiar stellar kinematics, as we would expect if the presence of ionized gas is the result of interactions and merging events that may affect also the stellar kinematics.

In our sample there are no one-to-one relationships between gaseous and stellar kinematical characteristics, and all possible combinations seem to be present: regular gaseous and star kinematics (for example, NGC 3607); or

TABLE 3
KINEMATICAL CHARACTERISTICS

Identification	Type	Distance	Stellar Kinematics	Gaseous Kinematics	Gas/Star Counter-Rotation?
NGC 3379......	NG	14.5	Regular	Regular	NO
NGC 3489......	S0/Sa	9.2	CR core?	Regular	NO
NGC 3607......	S0	14.7	Regular	Regular	NO
NGC 4105......	S0	34.9	Regular	Regular	YES
NGC 4472......	E1/S0	21.3	CR core	...	...
NGC 4636......	E0/S0	21.3	KDIC	Irregular	...
NGC 5044......	E0	52.2	KDIC	Irregular	...
NGC 5077......	S0	52.2	CR core	Regular	YES?
NGC 5813......	E1	34.9	KDIC?	Irregular	YES
NGC 5846......	S0	34.9	KDIC?	Irregular?	...
NGC 5898......	S0	44.3	CR core	Regular	YES
NGC 5903......	E3/S0	44.3	Regular	Irregular	...
NGC 6758......	E2	58.8	KDIC	Regular?	YES
NGC 6868......	E3/S0	48.6	CR core	Regular?	YES

NOTES.—Stellar kinematical profiles have been classified into three groups: Regular, CR core (counter-rotating core), or KDIC (kinematically decoupled inner component). Gas rotation curves are classified as Regular (including minor disturbances), or Irregular. Distance is in megaparsecs.

both irregular (as in NGC 5044); regular gaseous velocity curve together with a counter-rotating stellar core (NGC 5898); and finally chaotic gaseous kinematics coexisting with ordered stellar kinematics (NGC 4636, though it may have a decoupled central region as previously described).

Mehlert et al. (1998) present a list of the 17 galaxies with kinematically decoupled cores mentioned in the literature, which includes two of our galaxies. Here we find four new objects containing a counter-rotating stellar core (NGC 5077, NGC 5898, NGC 6868, NGC 3489), and four more with evidence for a kinematically distinct inner region (NGC 4636, NGC 5044, NGC 5846, NGC 6758).

We can conclude that, in the present sample of gas-rich galaxies, gas distributions which are irregular or chaotic both in spatial and velocity distributions, gaseous components kinematically decoupled from the stellar body, as well as peculiarities in the stellar kinematics, seem to be the rule rather than the exception.

These findings support the model in which the gas is accreted from outside the galaxy, rather than produced inside it. Irregular/chaotic gas velocity profiles indicate that in many cases the gas has not yet settled into the equilibrium configuration, and the accretion took place recently. The existence of different gaseous components is also a possibility, and they may be the result of multiple acquisition events. The accretion processes have probably left their signature in the stellar kinematics, either as a result of subsequent star formation, or the ingestion of the stellar component of the accreted object.

REFERENCES

Bender, R., Saglia, R. P., & Gerhard, O. E. 1994, MNRAS, 269, 785 (BSG)
Bertola, F., & Bettoni, D. 1988, ApJ, 329, 102
Bertola, F., Bettoni, D., Danziger, J., Sadler, E., Sparke, L., & de Zeeuw, T. 1991, ApJ, 373, 369
Bertola, F., Cinzano, P., Corsini, E. M., Rix, H.-W., & Zeilinger, W. W. 1995, ApJ, 448, L13
Binette, L., Magris, C. G., Stasinška, G., & Bruzual, A. G. 1994, A&AS, 292, 13
Buson, L. M., et al. 1993, A&AS, 280, 409
Dalle Ore, C., Faber, S. M., Jesus, J., Stoughton, R., & Burstein, D. 1991, ApJ, 366, 38
Davies, R. L., & Birkinshaw, M. 1988, ApJS, 68, 409 (DB)
de Vaucouleurs, G., de Vaucouleurs, A., Corwin, H. G. Jr., Buta, R. J., Paturel, H. G., & Fouqui, P. 1991, Third Reference Catalogue of Bright Galaxies (Austin: Univ. Texas) (RC3)
Efstathiou, G., Ellis, R. S., & Carter, D. 1982, MNRAS, 201, 975
Fabian, A. C. 1994, ARA&A, 32, 277
Ferrari, F., Pastoriza, M., Macchetto, D., & Caon, N. 1999, A&AS, 136, 269
Fisher, D., Illingworth, G., & Franx, M. 1995, ApJ, 438, 539
Fosbury, R. A. E., et al. 1982, MNRAS, 201, 991
Franx, M., Illingworth, G., & Heckman, T. 1989, ApJ, 344, 613 (FIH)
Goudfrooij, P. 1996, Ap&SS, 209, 400
Goudfrooij, P., Hansen, L., Jørgensen, H. E., & Nørgaard-Nielsen, H. U. 1994, A&AS, 105, 341

Heckman, T., Baum, S. A., vanBreugel, W. J. M., & McCarthy, P. 1989, ApJ, 338, 48
Kim, D.-W. 1989, ApJ, 346, 653
Kormendy, J. 1984, ApJ, 287, 577
Macchetto, D., Pastoriza, M., Caon, N., Sparks, W. B., Giavalisco, M., Bender, R., & Capaccioli, M. 1996, A&AS, 120, 463 (Paper I)
Mehlert, D., Saglia, R. P., Bender, R., & Wegner, G. 1998, A&A, 332, 33
Osterbrock, D. E. 1974, Astrophysics of Gaseous Nebulae (San Francisco: Freeman)
Pastoriza, M. G., Winge, C., Ferrari, F., Macchetto, D., & Caon, N. 2000, ApJ, 529, 866
Phillips, M. M., Jenkins, C. R., Dopita, M. A., Sadler, E. M., & Binette, L. 1986, AJ, 91, 1062
Plana, H., Boulesteix, J., Amram, Ph., Carignan, C., & Mendes de Oliveira, C. 1998, A&AS, 128, 75
Prugniel, Ph., Zasov, A., Busarello, G., & Simien, F. 1998, A&AS, 127, 117
Saglia, R. P., et al. 1993, ApJ, 567, 572
Shields, J. 1991, AJ, 102, 1314
Sparks, W. B., & Collier-Cameron, A. 1988, MNRAS, 232, 215
Sparks, W. B., Macchetto, D., & Golombek, D. 1989, ApJ, 345, 153
Statler, T. S., & Smecker-Hane, T. 1999, AJ, 117, 839
Zeilinger, W. W., et al. 1996, A&AS, 120, 257